Self-driven photo-polarized water molecule triggered graphene ultraviolet photodetector

Shisheng Lin[1,2,3*], Chang Liu[1], Yanghua Lu[1,2], Xutao Yu[1], Yi Zhang[4] and Can Wang[1]

[1]College of Information Science and Electronic Engineering, Zhejiang University, Hangzhou, 310027, P. R. China.

[2]Hangzhou Gelanfeng Technology Co. Ltd, Hangzhou, 310051, P. R. China.

[3]State Key Laboratory of Modern Optical Instrumentation, Zhejiang University, Hangzhou, 310027, P. R. China.

[4]Key Laboratory of Wide Bandgap Semiconductor Materials and Devices, HC Semitek Corporation, Yiwu, 322009, P. R. China.

Email: shishenglin@zju.edu.cn

[*]Corresponding author.

Keywords: Self-driven, polarized liquid, photodetector, graphene

Abstract

Water is widely distributed on earth and contributes more than 70% of the human body as recognized as the source of life. The moving water has been used as the energy source of generators, which provides one of main part of the energy source of the daily life. However, water is rarely used in information or electronic devices. Herein, we demonstrate the feasibility of polarized water triggered photodetector where the polarized water is sandwiched between graphene and semiconductor. Due to the polarization and depolarization process of water molecular under the drive of photogenerated carriers, a photo-sensitive current can be repeatably produced, resulting in a high-performance photodetector. The response wavelength of the detector can be finely tuned as a result of the free choice of semiconductors as there is no requirement of lattice match between graphene and the semiconductors. Under zero voltage bias, the responsivity and specific detectivity of Gr/NaCl (0.5 M)/N-GaN reaches values of 224.9 mA/W and 8.2×10^{12} Jones under 350 nm illumination. This study transfers the message that water can be used as high-performance photodetector in informative industries.

Introduction

In the traditional PN junction, the Fermi level difference between p-type and N-type semiconductors creates a built-in electric field that can block originally diffused carriers and reach equilibrium. These PN junctions can be used as photodetectors in which the photogenerated carriers of incident light excitation are separated by a built-in electric field to output electrical signals[1-3]. Gallium Nitride (GaN) as a representative wide bandgap have been widely used for semiconductor PN junction photodetector and light-emitting diodes own to superior chemical stability and radiation hardness[4, 5]. Graphene (Gr) was born as

a novel two-dimensional semiconductor with carrier multiplication and superconductivity due to strong electron-electron interactions and band-gapless[6-9]. Combining 2D materials and 3D semiconductors to form heterojunctions, Gr/GaN heterojunction has been widely reported for optoelectronic devices based on traditionally PN junction[10-12].

Water (W), which is composed of two hydrogen atoms and one oxygen atom, has gained many attentions as a creative lightweight in-situ energy, which can be applied to the field of Internet of Things (IOT)[13-15]. Electrolytes can interact with water molecules in many ways, which possible because water molecules are strongly responsive to electrostatic fields of simple ions, charged macro molecules such as polyelectrolytes, or polar groups. In our previous work[16, 17], the energy of low-energy, disordered water flow converted into continuous direct current has been demonstrated via introducing polarized water molecules as mobile dielectrics in dynamic diodes. However, the effect of photo-carriers in polarization process has been neglected. Combing with the photoelectric effect, aqueous electrolyte solutions can be used to construct solid-liquid photodetectors.

In this work, we uncover the mix-phased high-performance ultraviolet photodetector, which inserting polar liquid into the PN junction can generate persistent photo-polarized current under illumination. Under the action of the polar liquid chemical potential and the semiconductor Fermi level, the photogenerated electrons and holes will continuously move to the opposite sides of the polar liquid droplet. Under zero bias voltage, The Gr/NaCl (0.5 M)/N-GaN exhibits a responsivity (R) and detectivity (D^*) up to 224.9 mA/W and 8.2×10^{12} Jones with 350 nm. Our method reveals the polarizing properties of polar liquids in the photoelectric effect, bringing a novel and promising approach for converting input light

energy into sustained polarized electricity and providing an additional dimension into photodetection.

Results and Discussion

A three-dimensional (3D) schematic model of Gr/liquid/N-GaN photodetector is shown in Fig. 1a, where the polar liquid is sandwiched between Gr, N-GaN and insulating layer. To confirm the structural properties of related semiconductors, the typical Raman spectroscopy was recorded in Fig. 1b, the bottom panel shows the obvious characteristic positioned peaks at 568.53 and 738.33 cm^{-1} are corresponds to E_2 (high) and A_1 (LO) phonon modes of GaN and peak located at 534.42 cm^{-1} is corresponds to A_1 (TO) phonon mode[12]. The top panel shows the Raman spectra of Gr on Si/SiO_2 substrate, the peaks observed at 1592.3 and 2685 cm^{-1} can be attributed to G peak and 2D peak[18, 19]. Remarkably, the extremely weak D peak (1345 cm^{-1}) reveals high quality and limited defects of graphene[20]. The current and voltage (I-V) curves of the Gr/W/N-GaN and Gr/W/P-GaN under dark and 350 nm illumination are illustrated in Figure 1c, where two devices show rectification behavior in opposite directions. The current and time (I-T) curves of Gr/W/N-GaN photodetector under zero bias voltage with multiple cycles of light switching is shown in Figure 1d. Obviously, a spike current belonging to the transient polarization process appears at the moment of turning on the light, subsequently, photo-polarization current tends to be steady state. A smaller reverse spike appears at the turning off the light, which belongs to depolarization process. The transient and steady state photo-polarization current of Gr/W/N-GaN basically reached 4.8 μA and 1.5 μA. A control experiments are directly show the advantages of inserting polar liquids between the Gr and GaN in constructing high-performance self-driven photodetectors. As shown in Figure 1e, compared with traditional solid-

state Gr/N-GaN heterojunction photodetector (middle panel) and direct physical contact Gr/N-GaN structure without water (right panel), Gr/W/N-GaN photodetector (left panel) exhibits highly performance. This type of photodetector could have a good performance competitive with the traditional PN diodes-based photodetector. Notably, in conventional solid-state Gr/N-GaN heterojunction photodetectors, after excited by incident light, photogenerated carriers are separated by the built-in electric field and collected by external circuit. Therefore, transient photo-polarization current will not occur.

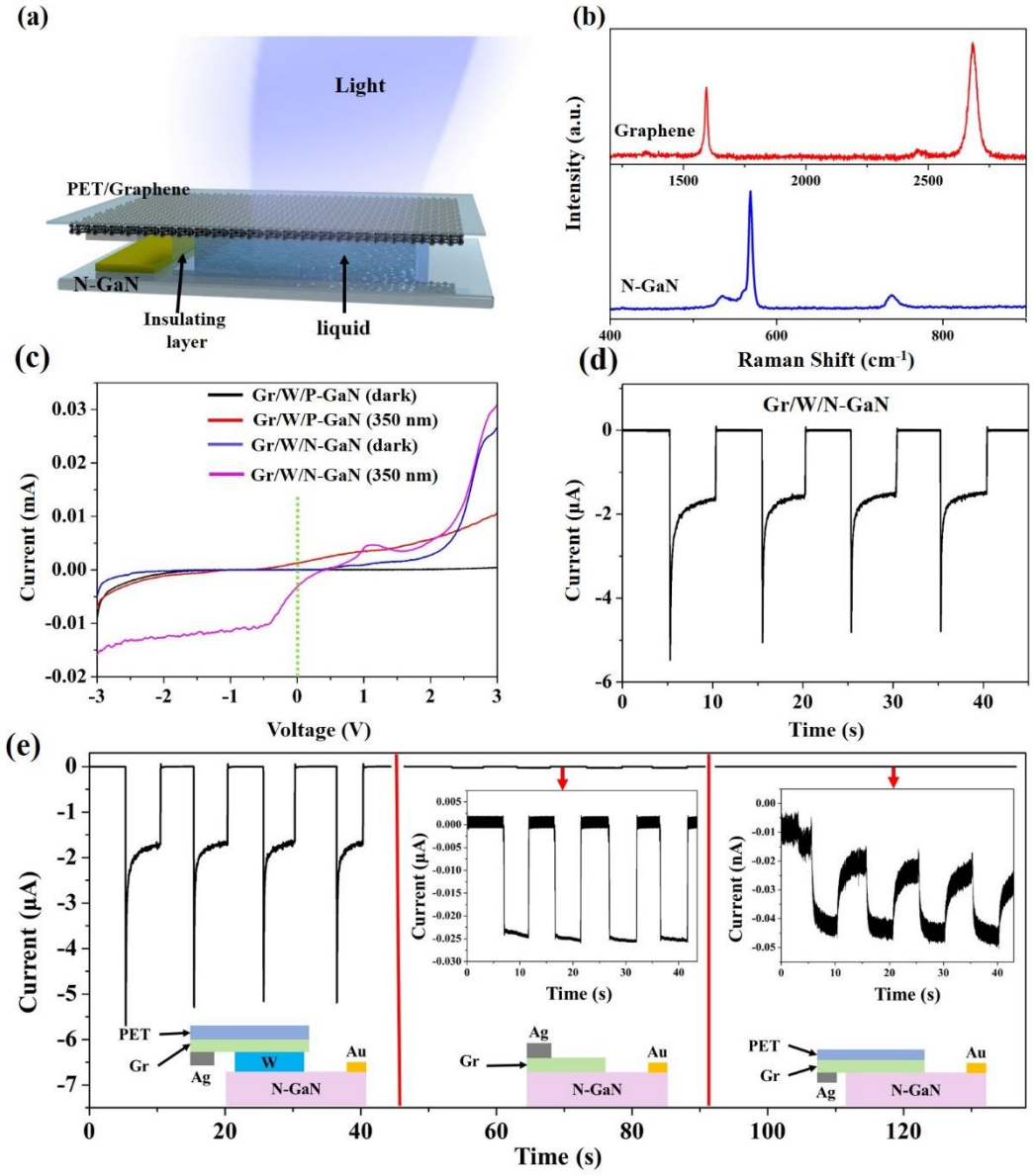

Figure 1. a) Schematic diagrams of device structure. b) Raman spectrum of bi-layer graphene on Si/SiO_2 substrate and N-GaN, respectively. c) I-V curves of the Gr/W/N-GaN and Gr/W/P-GaN photodetector under dark and 350 nm illumination. d) The photo-polarization current of Gr/W/N-GaN under 350 nm illumination with 261 μW/cm^2. e) The photo-polarization current of different device structures under same test conditions. The red arrow points to the enlarged view of photo-polarization current.

Notably, under the same test conditions, Gr/W/N-GaN and Gr/W/P-GaN exhibit different directional photocurrent. We explain the emergence of bipolar photocurrents from band structures physical mechanisms. The Fermi level of Gr after wet transfer is determined by $S = |\Delta E_f| \times 42 cm^{-1} eV^{-1}$[21], where S is the difference with the G peak relative to 1580 cm^{-1}, and ΔE_f is the difference with the graphene Fermi level relative to the Dirac point. Theoretically, the Dirac point of graphene is around 4.6[22]. The measured G peak locates at 1592.3 cm^{-1} from the Raman spectrum, and the work function of graphene is evaluated around 4.89 eV. Meanwhile, the work function of N-GaN and P-GaN is around ~4.0 eV and ~6.1 eV according to the doping of the Si and Mg[23, 24]. The work function of water can be estimated to 4.2 eV under standard atmospheric[25]. As indicated in Figure 2 (a and d), before contact, the water molecules is disordered state. After contact, Figure 2 (b and e), due to the work function difference, energy band gap alignment between GaN and Gr will be occurred. Meanwhile, the water molecules at the solid-liquid interface will be ordered polarized due to the Fermi level difference. As illustrated in Figure 2c and Figure 2f, under the excitation of light, the photogenerated carriers drift to the interface in large quantities, which polarizes many water molecules. As shown in Fig. 2c, the holes in N-GaN will accumulated at the interface between water/N-GaN, and the corresponding electrons in Gr will accumulate at the interface between Gr/water. Compared with Gr/W/N-GaN, the carrier

type at the interface of Gr/W/P-GaN devices are completely opposite. Meanwhile, the voltage and time (V-T) curves of Gr/W/N-GaN photodetector with different parallel resistances is shown in Figure S1. Obviously, the photogenerated voltage is well following with the switching light on/off, and rises with increasing shunt resistance. We further discuss the relationship between the number of graphene layers and the polarization current. It can be seen that the polarization photocurrent of double-layer graphene is larger than other samples (Figure S2), which might be due to the serious carrier recombination in multilayer graphene and makes it difficult to polarize more molecules to participate in charge transport.

Molecular polarization and photogenerated carrier coupling in polar liquids can efficiently generate photocurrents. In order to further confirm that the photocurrent originates from the polarization process, we use the non-polar liquid n-hexane as a medium to insert between Gr and N-GaN. The I-T curves of Gr/n-hexane/N-GaN device was shown in Figure S3. Clearly, this device does not generate photocurrent during optical switching process, confirming that the photocurrent is caused by the liquid polarization and photogenerated carrier coupling. Furthermore, we replaced the polar liquid with a salt solution of polar liquid, the photocurrent has been further improved. As indicated by Figure 3 (a, b and c), after replacing water with NaCl solution, the photo-polarization current is significantly improved under 350 nm on and off illumination. The transient and steady state photo-polarization current of Gr/NaCl/N-GaN reached 7.3 μA/3.7 μA, 7.6 μA/4.3 μA and 4.3 μA/2.6 μA under 350 nm irradiation, corresponding to Gr/NaCl (0.1 M)/N-GaN, Gr/NaCl (0.5 M)/N-GaN and Gr/NaCl (1.0 M)/N-GaN samples, respectively. Compared with the Gr/W/N-GaN, the salt ions lift up the conductivity of the water and also promote the interaction and ordered alignment of the

water molecular[26-28], thus increasing the performance of the photodetector inducing the maximum responsivity increased by 58.3%. Meanwhile, we found that the transient polarization current decreases significantly when the concentration of NaCl solution reaches 1.0 M, excessive ions will accumulate to the solid-liquid interface prior to the polarization of water molecules, and the electric field shielding weakens the steady state polarization photocurrent.

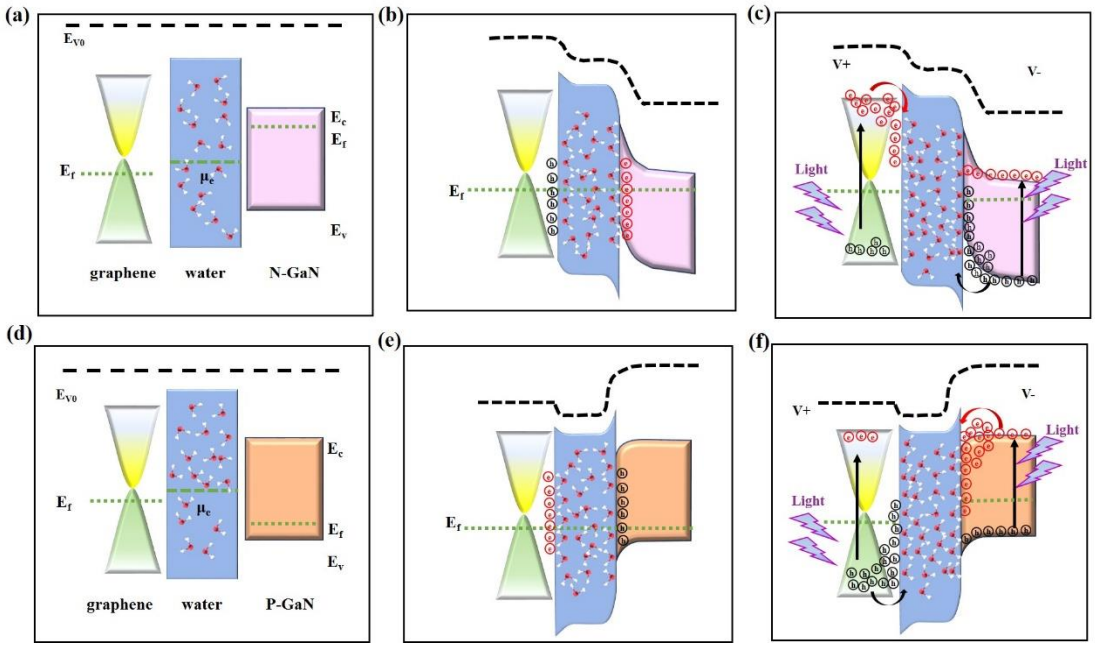

Figure 2. The band structures physical mechanisms of the Gr/W/N-GaN and Gr/W/P-GaN photodetector. a) and d) before contact, b) and e) after contact, c) and f) under light illumination.

To further exhibited the polarization mechanism more intuitively, we give the one switching cycle of Gr/NaCl (0.5M)/N-GaN photodetector in Figure 3d, and working mechanism in Figure 3 (e to h). After contact, different Fermi levels between materials induce polarization of water molecules at the interface, where oxygen atoms point to graphene and hydrogen atoms point to N-GaN[16]. And the Na^+ and Cl^- in the solution are attracted by different polarity charges and move to opposite directions (Figure 3e). As shown by step 1, the semiconductor is instantly excited by the irradiation, and a large number of photogenerated carriers will

move to the interface between the semiconductor and the liquid under the action of the built-in field, inducing the rapid accumulation of positive and negative ions in the salt solution and molecular polarization at the interface. The movement of the carriers will generate a higher photo-polarization current, as indicated by the process of step 1 in Figure 3d. In the next step (Figure 3g), the polarization current tends to be stable with more water molecules are polarized and ions move to the solid-liquid interface, as indicated by the process of step 2 in Figure 3d. As shown in step 3 of Figure 3d, after the light source is turned off, since the photo-induced carriers instantaneously relax and recombine with the lattice defects immediately, most of the water molecules are depolarized and result in a negative current output. The physical map changes from Figure 3g to Figure 3h.

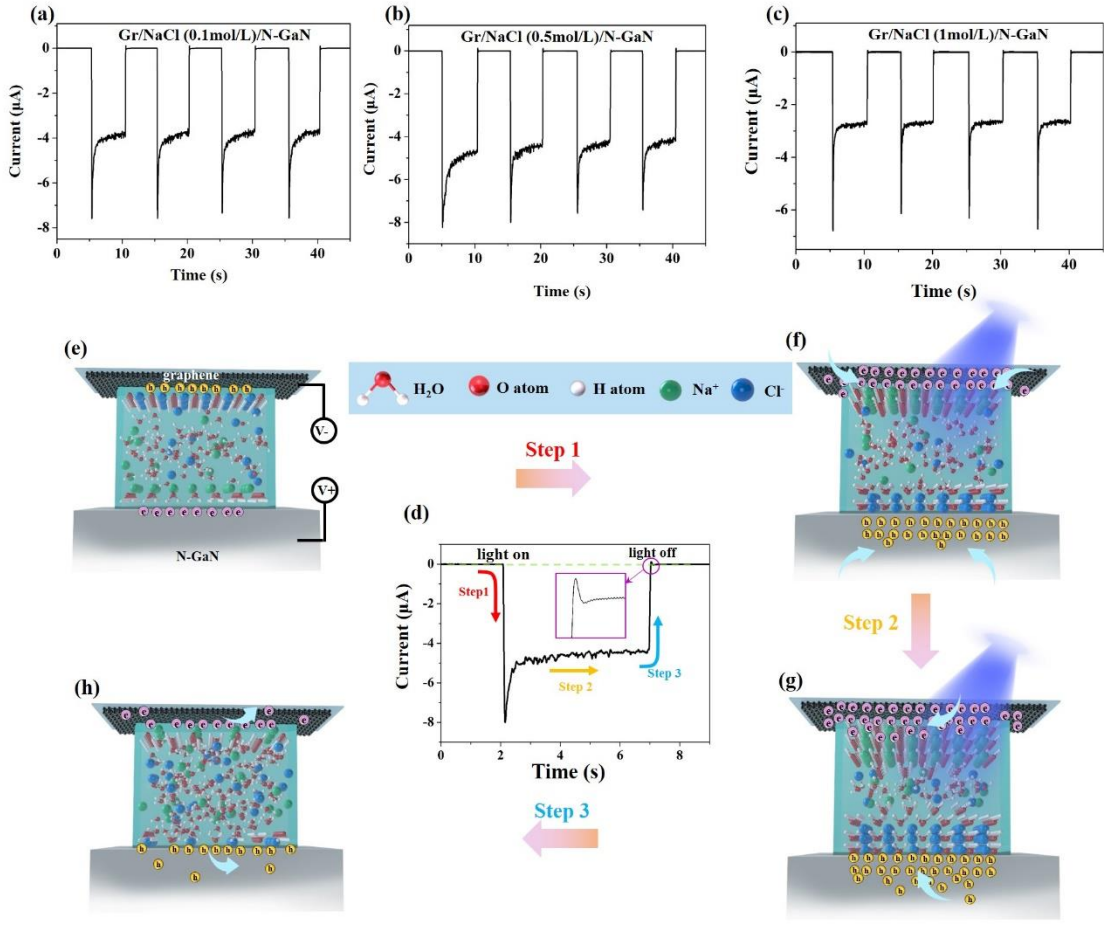

Figure 3. The photo-polarization current of a) Gr/NaCl (0.1 M)/N-GaN, b) Gr/NaCl (0.5 M)/N-GaN and c) Gr/NaCl (1 M)/N-GaN samples under 350 nm illumination with 261 μW/cm^2. Working mechanism of the Gr/NaCl (0.5 M)/N-GaN photodetector under light illumination. d) Time-current curves of device. e) Equilibrium state of Gr/NaCl (0.5 M)/N-GaN photodetector after the contact. f) Photocarrier accumulation induced the polarization state after the semiconductor excited. g) Continuously stable polarization state induced by accumulation under stable illumination. h, Depolarization process after turning off the light.

The self-powered I-T curves of the Gr/NaCl (0.5 M)/N-GaN photodetector under 350 nm with different optical intensities of 66.1, 152.5, 235.9, 314.5, 385.3, 452.9 and 518.9 μW/cm^2 are shown in Fig. 4a, respectively. The transient/steady state photo-polarization current increases with increasing optical power density, which is due to more photo-induced charge carriers are coupled to water molecules and ions under higher intensities of light. It's worth noting that the polarized current increases gradually without a saturation, which means prepared mis-phase photodetector could have a good performance competitive with the traditional solid-state photodetector. To further evaluate the overall performance of the photodetector, R and D* are indispensable parameters, representing the ability to convert unit optical power into photo-current and detect weak signal. The R can be determined by the following formula (1):

$$R = \frac{I_L - I_D}{PS} \quad (1)$$

where I_L is the transient/steady state photo-polarization current, I_D is the dark current, P is the incident optical power density. S is the effective illumination area of Gr/NaCl/N-GaN. Meanwhile, D* can be determined by the following formula (2):

$$D^* = \frac{\sqrt{S} * R}{\sqrt{2qI_D}} \quad (2)$$

where S represents the active work area of detector, q represents the

charge constant. Fig. 4b shows the R and D^* of transient photo-polarization current for Gr/NaCl (0.5 M)/N-GaN photodetector as a function of incident light power density. The maximum R and D^* are reaches values of 224.9 mA/W and 8.2×10^{12} Jones under zero bias voltage. Fig. 4c shows the R and D^* of steady state photo-polarization current for Gr/NaCl (0.5 M)/N-GaN photodetector as a function of incident light power density. The maximum R and D^* are reaches values of 140.2 mA/W and 5.3×10^{12} Jones under zero bias voltage.

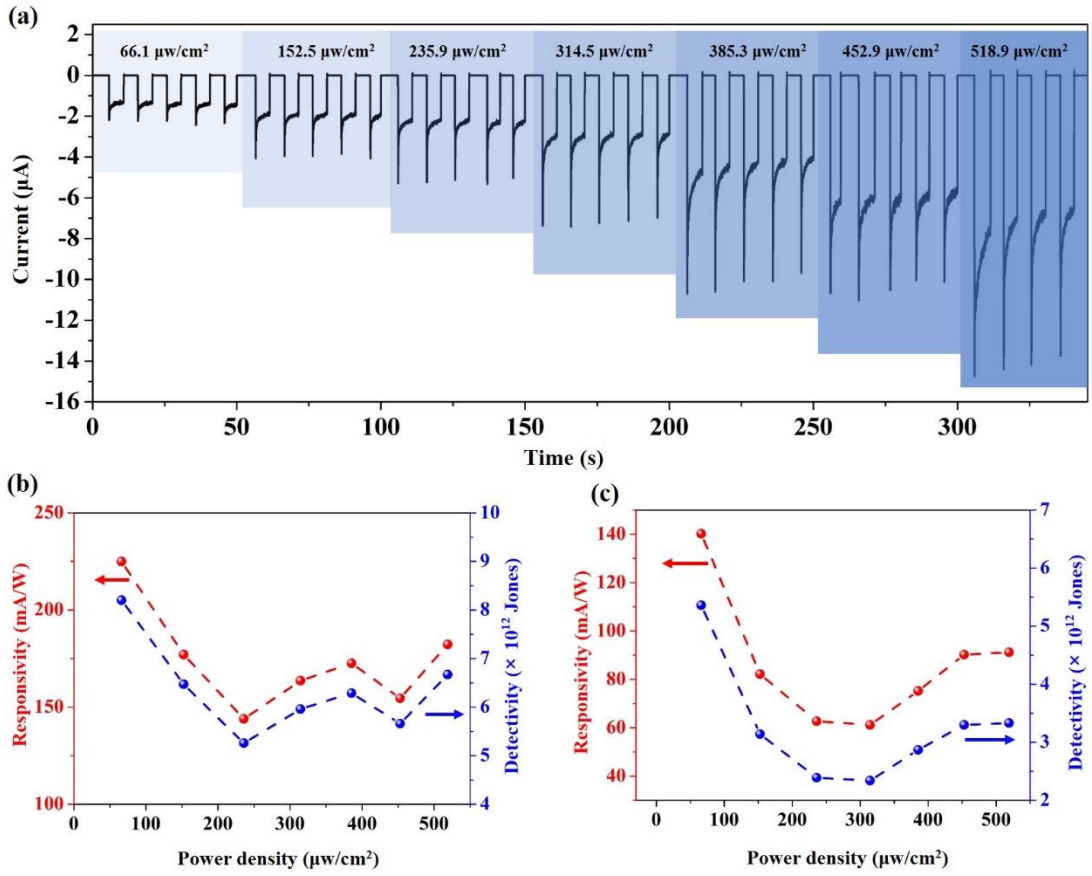

Figure 4. a) The photo-polarization current of the Gr/NaCl (0.5 M)/N-GaN photodetector under 350 nm with different optical power intensities. Responsivity and detectivity of b) transient photo-polarization current and c) steady photo-polarization current as a function of incident optical power intensity under zero bias.

Figure 5a reveals the curve of photo-polarization current as a function of incident wavelength. The corresponding power density of different wavelength are shown in Figure S4. The photo-polarization current

increases significantly with the increase of the incident wavelength and reaches the maximum at 355 nm, which is related with the absorption capacity of the device. There is also a corresponded photo-polarized current response in the solar blind region, however, photogenerated carriers excited by larger photon energies at deeper positions within the semiconductor will recombine rapidly. The UV-Vis absorption spectra of the N-GaN exhibits a steep absorption edge around 360 nm (Figure S5), which corresponds to its bandgap, and has negligible absorption in the visible region. The typical spectral responses of Gr/NaCl (0.5 M)/N-GaN photodetector are exhibited in Fig. 5b. The UV-visible rejection ratio defined as the ratio of the responsivity at 330 and 400 nm is about 1.4×10^2.

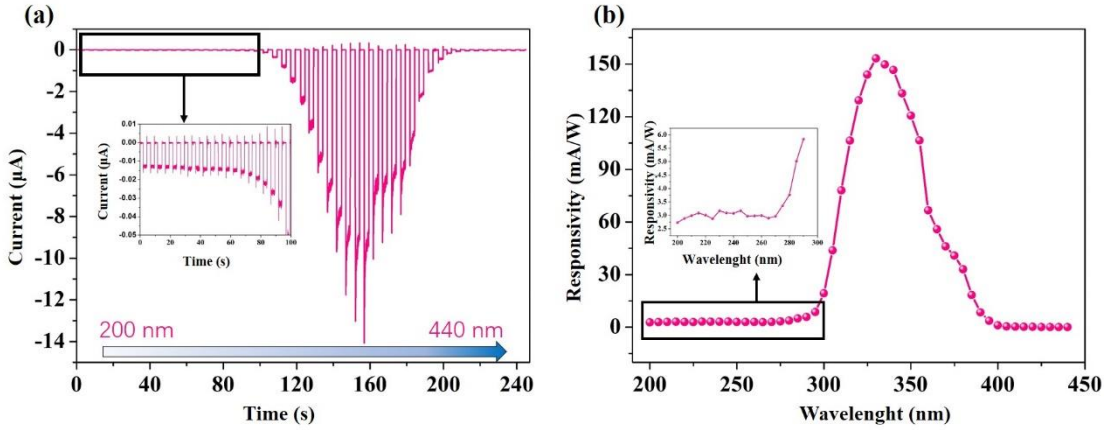

Figure 5. a) Time-resolved photo-polarization current of the Gr/NaCl (0.5 M)/N-GaN photodetector under different wavelength (200 nm to 440 nm, step with 5 nm). b) Responsivity of steady photo-polarization current as a function of wavelength under zero bias.

Conclusions

In conclusion, photo-induced liquid polarization ultraviolet photodetector was realized by integrated polar liquid and semiconductor. Photogenerated carrier coupled to water molecules and ions has been investigated thoroughly. As a comparison, we confirm that the liquid is

not in a conducting state when illuminated, and the current is caused by dynamic polarization process of the liquid sandwiched between the semiconductors with different Fermi levels. Under 350 nm illumination with 66.1 μW/cm^2 power density, the responsivity and detectivity of transient photo-polarized current and steady state photo-polarized current in Gr/NaCl (0.5 M)/N-GaN reach values of 224.9 mA/W and 8.2×10^{12} Jones and 140.2 mA/W and 5.3×10^{12} Jones, respectively. This work integrates polar liquids into heterojunctions, which is expected to provide a new direction for mixed-phase optoelectronic devices by optimizing polar liquid species and additives.

Experimental Section

Device fabrication and measurement: Deionized water, containing a few foreign ions σ < 20 μS/cm, was obtained by lab water purification system (Heal Force RWD-1). n-hexane in this work were analytical grade without further purification. NaCl was purchased form Sinopharm chemical reagent Co., Ltd. The epitaxial P-GaN film with Mg concentration ~5×10^{19} cm^{-3}, epitaxial N-GaN film with Si concentration ~6×10^{19} cm^{-3} and 2.2 μm undoped GaN and 540 nm N-GaN was grown on a sapphire substrate by metal organic chemical vapor deposition method (MOCVD, HC SemiTek). The GaN substrate was ultrasonically cleaned by acetone, isopropanol, ethanol and deionized water for 10 minutes. Ni (15 nm)/Au (90 nm) contact was by thermally evaporated onto one side of substrates successively. Subsequently, a 150 μm thick square polyimide tape with a 0.3 × 0.5 mm window was transferred onto P-GaN or N-GaN. The graphene was synthesized by CVD method according to our previous work[19]. Utilizing polyethylene terephthalate (PET) (130 μm) as the support film, the graphene was transferred to the

PET surface by wet transfer method[29, 30]. Finally, the PET/Gr was transferred to a window insulating layer made by PI tape.

Characterization analysis: The I-V curves were measured by a Keithley 2400 source meter and I-T curves were carried out by Keithley 6514 source meter and DMM6500 multimeter. Photo-current test was measured by a detecting system consisting of a Xe lamp (SOFN Instruments Co., Ltd. 7ILX500C) and monochromator (SOFN Instruments Co., Ltd. 7ISW15). Raman spectra were measured by a Reinishaw system with an excitation laser of 532 nm. Power density of different wavelength was detected by an S120 VC optical power meter by THOR-LABSU. UV-vis absorption spectra of GaN was recorded by UV-vis spectrophotometer (NatureSci Technologies Corporati Lambda950) in the range of 300-1000 nm.

Author Contributions

S. Lin designed the experiments, participated the experiments, analyzed the data, conceived the study, and wrote the paper. C. Liu assisted to design and carry out the experiments, discuss the results. Y. Lu, Yi Zhang, X. Yu and C. Wang discussed the results and assisted with experiments. All authors contributed to the preparation of the manuscript.

Acknowledgements

S.S.L. thanks the support from the National Natural Science Foundation of China (No. 51202216, 51502264, 61774135, and 51991342), Distinguished Youth Fund of Zhejiang Natural Science Foundation of China (LR21F040001), and Special Foundation of Young Professor of Zhejiang University (2013QNA5007). Y.H.L. thanks the support from the

China Postdoctoral Science Foundation (2021M692767).

Conflict of Interest

The authors declare no conflict of interest.

Reference

[1] A. Ishii, T. Miyasaka, Science Advances 2020, 6, eabd3274.
[2] C. Fuentes-Hernandez, W.-F. Chou, T. M. Khan, L. Diniz, J. Lukens, F. A. Larrain, V. A. Rodriguez-Toro, B. Kippelen, Science 2020, 370, 698.
[3] I. Nikitskiy, S. Goossens, D. Kufer, T. Lasanta, G. Navickaite, F. H. L. Koppens, G. Konstantatos, Nature Communications 2016, 7, 11954.
[4] S. K. Jain, M. X. Low, P. D. Taylor, S. A. Tawfik, M. J. S. Spencer, S. Kuriakose, A. Arash, C. Xu, S. Sriram, G. Gupta, M. Bhaskaran, S. Walia, ACS Applied Electronic Materials 2021, 3, 2407.
[5] W. Song, J. Chen, Z. Li, X. Fang, Advanced Materials 2021, 33, 2101059.
[6] Y. Lin, Q. Ma, P.-C. Shen, B. Ilyas, Y. Bie, A. Liao, E. Ergeçen, B. Han, N. Mao, X. Zhang, X. Ji, Y. Zhang, J. Yin, S. Huang, M. Dresselhaus, N. Gedik, P. Jarillo-Herrero, X. Ling, J. Kong, T. Palacios, Science Advances 2019, 5, eaav1493.
[7] A. Tomadin, S. M. Hornett, H. I. Wang, E. M. Alexeev, A. Candini, C. Coletti, D. Turchinovich, M. Kläui, M. Bonn, F. H. L. Koppens, E. Hendry, M. Polini, K.-J. Tielrooij, Science Advances 2018, 4, eaar5313.
[8] Y. Saito, J. Ge, K. Watanabe, T. Taniguchi, A. F. Young, Nature Physics 2020, 16, 926.
[9] C. Liu, Y. Lu, R. Shen, Y. Dai, X. Yu, K. Liu, S. Lin, Nano Energy 2022, 95, 106977.
[10] Y. Lu, Z. Wu, W. Xu, S. Lin, Nanotechnology 2016, 27, 48lt03.
[11] Z. Wu, Y. Lu, W. Xu, Y. Zhang, J. Li, S. Lin, Nano Energy 2016, 30, 362.
[12] C. Liu, Y. Lu, X. Yu, R. Shen, Z. Wu, Z. Yang, Y. Yan, L. Feng, S. Lin, Carbon 2022, 197, 192.
[13] S. Tang, J. Gong, Y. Shi, S. Wen, Q. Zhao, Nature Communications 2022, 13, 3227.
[14] E. J. Lundgren, D. Ramp, J. C. Stromberg, J. Wu, N. C. Nieto, M. Sluk, K. T. Moeller, A. D. Wallach, Science 2021, 372, 491.
[15] L. Su, J. Mosquera, M. F. J. Mabesoone, S. M. C. Schoenmakers, C. Muller, M. E. J. Vleugels, S. Dhiman, S. Wijker, A. R. A. Palmans, E. W. Meijer, Science 2022, 377, 213.

[16] Y. Yan, X. Zhou, S. Feng, Y. Lu, J. Qian, P. Zhang, X. Yu, Y. Zheng, F. Wang, K. Liu, S. Lin, The Journal of Physical Chemistry C 2021, 125, 14180.
[17] Y. Lu, Y. Yan, X. Yu, X. Zhou, S. Feng, C. Xu, H. Zheng, Z. Yang, L. Li, K. Liu, S. Lin, Research 2021, 2021, 7505638.
[18] X. Li, S. Lin, X. Lin, Z. Xu, P. Wang, S. Zhang, H. Zhong, W. Xu, Z. Wu, W. Fang, Optics Express 2016, 24, 134.
[19] S. Feng, B. Dong, Y. Lu, L. Yin, B. Wei, J. Wang, S. Lin, Nano Energy 2019, 60, 836.
[20] Y. Lu, R. Shen, X. Yu, D. Yuan, H. Zheng, Y. Yan, C. Liu, Z. Yang, L. Feng, L. Li, S. Lin, Advanced Science, n/a, 2200642.
[21] A. Das, S. Pisana, B. Chakraborty, S. Piscanec, S. K. Saha, U. V. Waghmare, K. S. Novoselov, H. R. Krishnamurthy, A. K. Geim, A. C. Ferrari, A. K. Sood, Nature Nanotechnology 2008, 3, 210.
[22] S. Sarkar, E. Bekyarova, R. C. Haddon, Accounts of Chemical Research 2012, 45, 673.
[23] A. P. Herman, L. Janicki, H. S. Stokowski, M. Rudzinski, E. Rozbiegala, M. Sobanska, Z. R. Zytkiewicz, R. Kudrawiec, Advanced Materials Interfaces 2020, 7, 2001220.
[24] S. K. Jain, R. R. Kumar, N. Aggarwal, P. Vashishtha, L. Goswami, S. Kuriakose, A. Pandey, M. Bhaskaran, S. Walia, G. Gupta, ACS Applied Electronic Materials 2020, 2, 710.
[25] F. Maier, M. Riedel, B. Mantel, J. Ristein, L. Ley, Physical Review Letters 2000, 85, 3472.
[26] Y. Chen, H. I. Okur, N. Gomopoulos, C. Macias-Romero, P. S. Cremer, P. B. Petersen, G. Tocci, D. M. Wilkins, C. Liang, M. Ceriotti, S. Roke, Science Advances 2016, 2, e1501891.
[27] H. I. Okur, Y. Chen, D. M. Wilkins, S. Roke, Chemical Physics Letters 2017, 684, 433.
[28] H. I. Okur, C. I. Drexler, E. Tyrode, P. S. Cremer, S. Roke, The Journal of Physical Chemistry Letters 2018, 9, 6739.
[29] Y. Lu, S. Feng, Z. Wu, Y. Gao, J. Yang, Y. Zhang, Z. Hao, J. Li, E. Li, H. Chen, S. Lin, Nano Energy 2018, 47, 140.
[30] H. Zhong, Z. Wu, X. Li, W. Xu, S. Xu, S. Zhang, Z. Xu, H. Chen, S. Lin, Carbon 2016, 105, 199.